# Model-based view planning

Scott, William



https://doi.org/10.4224/5763577

National Research Council Canada
Conseil national de recherches Canada

Institute for Information Technology
Institut de technologie de l'information

NRC · CNRC

# *Model-Based View Planning* *

Scott, W.R.
March 2005

* published as NRC/ERB-1125. March 31, 2005. 18 pages. NRC 47448.



Canada

National Research Council Canada
Conseil national de recherches Canada

Institute for Information Technology
Institut de technologie de l'information

ERB-1125

NRC·CNRC

# Model-Based View Planning

Scott, W.R.
March 2005



Canada

NRC 47448

# Model-Based View Planning

William R. Scott†

† Computational Video Group,
National Research Council of Canada, Ottawa,
Canada, K1A 0R6
william.scott@nrc-cnrc.gc.ca

## Abstract

This paper presents a model-based view planning approach for automated object reconstruction or inspection using laser scanning range sensors. Quality objectives and performance measures are defined. Camera and positioning system performance is modeled statistically. A theoretical framework is presented. The method is applicable to a broad class of objects with reasonable geometry and reflectance properties. Sampling of object surface and viewpoint space is characterized, including measurement noise and pose error effects. The technique is generalizable for common range camera and positioning system designs.

## 1 Introduction

***Overview*** Laser range sensors [4] are widely used for high quality 3D object reconstruction and inspection. These processes involve planning views, physically altering the object-sensor pose, taking scans, registering the geometric data in a common reference frame and integrating range images into a non-redundant model. Efficiencies could be achieved through automation, yet the view planning component remains an open problem despite two decades of research. We believe this is due to over-simplification of the task. While view planning may appear straight forward, numerous factors influence the outcome, including subtle details of sensor and positioning system performance plus wide variations in object shape complexity and surface properties.

***Imaging Environment*** The imaging environment involves a triangulation-based range camera (e.g. Figure 1), positioning system, fixtures and an object. Modern range cameras are capable of precise, dense, high speed, non-contact range measurements [6]. However, the range measurement technique [7] has implications for view planning for high precision modeling and inspection. The optical baseline is significant with respect to the stand-off distance, resulting in coverage shadow zones (Figure 2). Field of view


Figure 1: NRC Range Camera

(FOV) and depth of field (DOF) are limited. Measurement precision and sampling density are non-uniform within the frustum. Further, measurement is subject to random non-isotropic geometric noise [3] and several artifact phenomena [12]. Due to dynamic range limitations, contemporary range sensors have difficulty with highly absorbent or reflective material.

Imaging all sides of an object requires multiple viewing perspectives. Thus, a positioning system is needed to move the sensor, the object or both. Positioning inaccuracies degrade view planning performance. Sensor pose is limited by the degrees of freedom and range of motion of the positioning system. Generalized viewpoints $(\mathbf{v}, \lambda_\mathbf{s})$ [38] associate a camera configuration $\lambda_\mathbf{s}$ with each sensor pose $\mathbf{v}$. Viewpoint space $V$ is the set of generalized viewpoints defined by the range and sampling of these parameters. Surface space $S$ is a set of 3D points. Fixtures, the positioning system and other structures in imaging workspace $I$ introduce occlusion and collision avoidance issues.

***View Planning Problem (VPP)*** Stated informally, the VPP is - "For a given imaging environment and target object, find a suitably short view plan $N$ satisfying the specified reconstruction/inspection goals and achieve this within an acceptable computation time." The VPP involves reasoning about object surface space $S$, viewpoint space $V$ and imaging workspace $I$. The problem's complexity is apparent from the high dimensionality of $S$, $V$ and $I$. Refer to Scott et al.[32] for an in-depth discussion and survey.

***View Planning Requirements*** Development of the algorithm described in this paper was driven by a set of view planning requirements derived from examination of the state-of-the-art and consideration of nature of the problem to be addressed [32]. In summary, a view planning algorithm should:
- incorporate quantified model quality objectives,
- be generalizable to other imaging technologies,
- handle generalized viewpoints,
- provide overlap for integration and registration,
- be robust to sensor and positioning errors,
- be competitive with human operator efficiency,
- be self-terminating,
- require limited a priori knowledge,
- handle a wide range of object shapes and topologies,
- handle a wide range of object material properties,
- model the shape of the sensor frustum,
- include shadow effects,
- model measurement variation within the frustum, plus common sensing artifacts,
- handle unconstrained pose space,
- handle positioning system limitations and
- model pose error over the imaging workspace.

No existing method fully meets these requirements [32]. This paper presents a specification-driven, model-based technique satisfying most of these criteria and advancing performance on the main open view planning issues - efficiency, accuracy and robustness.

***Outline*** The remainder of this paper is organized as follows. Sections 2 and 3 describe the algorithm and provide a theoretical framework. Sections 4 and 5 analyze discretization of surface and viewpoint space while section 6 addresses pose error. Experimental results are presented in section 7. Section 8 concludes the paper and discusses issues for future work.

# 2 Modified Measurability Matrix Algorithm

## 2.1 Multi-Stage Model-Based View Planning

Object reconstruction requires both scene exploration and precise measurement. Traditional view planning methods [32] attempt these functions simultaneously. They repetitively take an image, acquire new information, augment a partial scene model and select the next-best-view (NBV). The strategy is inherently suboptimal as early selections cannot be revoked.

View planning for inspection [39, 21] is intrinsically model-based as it starts with a CAD model. Some contour following schemes [36, 17] utilize an initial low resolution object scan for subsequent view planning purposes. Garcia [15] first attempts to sample most of the object using an occlusion edge method, leaving computationally expensive visibility analysis to a second hole-filling stage.

Our approach, multi-stage model-based view planning [28], separates scene exploration from precise measurement. We begin with a rapid, preprogrammed exploration phase to acquire a sparsely-sampled *exploratory* or *rough model*. This approximate representation is used to plan a precise, dense scanning phase to acquire the desired high quality reconstruction, the *fine model*. Exploiting scene knowledge embedded in the rough model, the precision measurement phase can use optimized revocable viewpoint selection strategies. Efficient sampling of surface and viewpoint space is achievable due to the high degree of intrinsic redundancy. Sensing physics provide important clues for viewpoint optimization. Consequently, we follow a generate and test procedure concentrating measurability estimation on a coarse surface representation with respect to a modest number of well-chosen candidate viewpoints. In practical implementation of a fully automated system, we anticipate a third problem identification and resolution phase would be required to handle any residual model deficiencies[1]. This paper focuses on the second phase, which we believe is the key to view plan automation for high precision modeling and inspection.

## 2.2 Specification-Driven Reconstruction and Inspection

Specification-driven (or "performance-oriented") [26, 23] view planning starts with explicit, quantified quality objectives in a *model specification* and finishes with quantified performance measures. Currently, our model specification applies quantitative requirements for measurement precision and sampling density uniformly across the object with an implicit full coverage requirement. In some applications, it may be appropriate to limit coverage to specified regions or to apply non-uniform measurement criteria. Quantified output measures include view plan quality and efficiency (Section 2.4). The approach requires good system models: (1) a sensor model describing camera and frustum ge-

[1] Such a problem identification and resolution phase would realistically be required for any production view planning system with high quality measurement objectives.

ometry and characterizing measurement performance within the calibrated region and (2) a positioning system model describing the degrees of freedom, range of motion and positioning performance within the calibrated movement envelope.

Cowan and Kovesi [11] use a constraint satisfaction approach for sensor pose. Tarabanis et al [38] synthesize views for intensity cameras based on a task specification, models for scene geometry and sensor and illumination optics. Soucy et al [36] digitize an object's surface to a prescribed sampling density using contour following. Prieto [21] sets CAD-based inspection criteria based on range sensor performance characterization. A number of authors consider grazing angle as a subjective quality factor. Otherwise, most view planning research has been implicitly limited to full surface observation.

## 2.3 Measurability Matrix

Our basic data structure is a measurability matrix $\mathbf{M} = [m_{ij}]$. Rows span discretized surface space $S$ (vertices of the rough model mesh) while columns span discretized viewpoint space $V$. The computational complexity of the original measurability matrix approach by Tarbox [39] was prohibitive, given the span of the discretized variables. Our modification applies objective output requirements (measurement precision and sampling density) in lieu of subjective grazing angle constraints. We also mathematically model sensor and positioning system performance, optimize surface and viewpoint space sampling prior to computing $\mathbf{M}$ and address sampling and pose error impacts. Both binary and analogue measurability matrices can be defined. The binary version is more compact and best suits the needs of the current work.

## 2.4 Terminology and Performance Measures

*Measurability matrix element* $m_{ij}$ is a binary estimate of the measurability of a rough model surface point $\mathbf{s}_i$ from viewpoint $\mathbf{v}_j$, subject to the following tests:
a. *Frustum occupancy* - $\mathbf{s}_i$ must lie within the world space sensor frustum defined by $\mathbf{v}_j$.
b. *Visibility* - $\mathbf{s}_i$ must be visible to the optical source and receiver positions defined by $\mathbf{v}_j$.
c. *Specification-compliance* - The estimated measurement precision and sampling density for $\mathbf{s}_i$ as sampled by $\mathbf{v}_j$ must be within specification.

The *measurability of a single viewpoint* $m(\mathbf{v}_j)$ or, equivalently a range image, is the ratio of the coverage $|S_j|$ of that viewpoint relative to the size of the surface patch as a whole $|S|$. That is $m(\mathbf{v}_j) = |S_j|/|S|$.

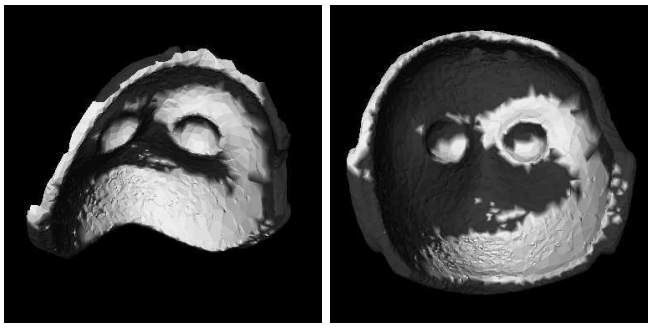

Figure 2: Measurability Projection: (L) Sensor Boresight View, (R) Orthogonal View ; Black - unmeasured, White - samples meeting measurement criteria

Similarly, the *composite measurability* of a set of viewpoints is the ratio of the joint coverage of those viewpoints to the size of the surface patch - $m(\mathbf{v}_1, \mathbf{v}_2, \ldots, \mathbf{v}_k) = |S_1 \cup S_2 \cup \ldots \cup S_k|/|S|$.

A *measurability projection* is a 2D projection of a labeled rough or fine model mesh whose vertices are encoded with their binary measurability. In this paper, binary measurability projections are shaded black for unmeasured and white for measured in compliance with the model specification. Regular grey scale shading is superimposed to convey shape. The example at Figure 2 represents two views of one range sampling of the rear of the Tsimshian stone mask object described in Section 7. Shadowing and surface inclination effects on measurability can be observed[2].

The view planning algorithm operates on *estimated measurability* of viewpoints based on an approximate exploratory scene model. When the view plan is executed by a real sensor against the real object or by a sensor model against a simulated fine model, the result is *verified measurability.*

The following metrics evaluate view planning algorithm performance [32]. *View plan quality* is determined by its composite verified measurability $m_v$. The goal is $m_v = 1.0$.

*View plan efficiency* is the length of the generated view plan relative to the optimum i.e. $e_v = n_{Opt}/n$, where $n = |N|$. As determining $n_{Opt}$ may be impractical for complex tasks, a surrogate is the length of the best solution $n_{Best}$ found thus far amongst all tech-

[2]The patchy sampling observed in this example is commonly seen in range images. Most conventional view planning techniques would have difficulty handling such discontinuous data.

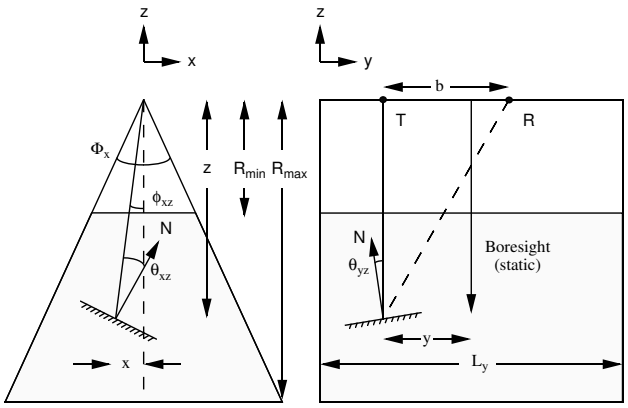


Figure 3: Line-scan Range Camera Geometry

niques examined for the same task i.e. $n_{Opt} \approx n_{Best}$. The goal is $e_v = 1.0$.

*View plan computational efficiency* measures are computational complexity and execution time on a defined platform.

## 2.5 Sensor Performance Model

**Range Camera Geometry** We have modeled the performance of several range camera designs, including line and raster scanning modes. The imaging geometry of a common configuration, the line-scan camera, is shown at Figure 3. By convention, the camera axis defines the negative z-axis. Scanning occurs optically in the x-z plane, where $\phi_{xz}$ is the instantaneous laser scan angle, and mechanically in the y-z plane by physical movement of the camera along its y-axis. The frustum is defined by $\Phi_x$ (x-z plane angular field of view), $L_y$ (y-z plane linear scan length) and $R_{min}$ and $R_{max}$ (minimum and maximum scanning ranges). Separated by the optical baseline $b$, the transmitter (laser) and receiver (detector) are housed in a single physical unit and move in unison.

**Measurement Precision** We estimate the statistics of post-calibration, residual random measurement error of the range sensor as $\hat{\sigma}_x = C_x z$, $\hat{\sigma}_y = C_y z$, $\hat{\sigma}_z = C_z z^2$. In the foregoing, $\hat{\sigma}_x, \hat{\sigma}_y, \hat{\sigma}_z$ are standard deviation estimated geometric noise components. Coefficients $(C_x, C_y, C_z)$ are derived from curve fitting calibration data (e.g. [13]). As noise along the sensor boresight predominates, we use $\hat{\sigma}_z$ as a surrogate for measurement precision. This is further modified by an experimentally-based grazing angle model[3]. Incidence angle effects are most noticeable in the plane of triangulation, the yz-plane, where they generally follow an inverse cosine relationship up to a cut-off angle $t_{yz}$ due to distortion of the shape of the envelope of received energy on the camera detector. There is no noticeable inclination effect in the scanning plane up to a cut-off angle $t_{xz}$, at which point the received energy drops below threshold. Typical thresholds are $t_{yz} = 60°$ and $t_{xz} = 70°$. Thus, we model estimated precision as follows, where $U(\theta)$ is the unit step function.

$$\hat{\sigma}_z = \frac{C_z z^2}{\cos\theta_{yz}\,[1 - U(|\theta_{yz}| - t_{yz})]\,[1 - U(|\theta_{xz}| - t_{xz})]}. \quad (1)$$

**Sampling Density** We use a conservative chord-based estimate for sampling density $\hat{\rho}_z$, where $\delta x$ and $\delta y$ are x- and y-axes sampling intervals. Then,

$$\hat{\rho}_z = \frac{1}{\delta x^2 + \delta y^2} \quad (2)$$

$$\text{where } \delta x = R_{xz}\frac{\Phi_x}{N_x - 1}\frac{1}{\cos\theta_{xz}} \quad (3)$$

$$\text{and } \delta y = \frac{L_y}{N_y - 1}\frac{1}{\cos\theta_{yz}}. \quad (4)$$

In Equation 3, $R_{xz} = z/\cos\phi_{xz}$ is the slant range, $\Phi_x/(N_x - 1)$ is the angular sampling interval and $1/\cos\theta_{xz}$ is the inclination effect in the x-z plane. In Equation 4, $L_y/(N_y - 1)$ is the linear sampling interval and $1/\cos\theta_{yz}$ is the inclination effect in the y-z plane. Image size is $N_x$-by-$N_y$ samples. Combining these expressions, the estimated sampling density becomes

$$\hat{\rho}_z = \frac{(N_x - 1)^2(N_y - 1)^2\cos^2\theta_{xz}\cos^2\theta_{yz}}{{R_{xz}}^2{\Phi_x}^2(N_y - 1)^2\cos^2\theta_{yz} + {L_y}^2(N_x - 1)^2\cos^2\theta_{xz}}. \quad (5)$$

## 2.6 Positioning System Error Model

A variety of positioning systems are in common usage, covering a wide range of accuracy, including co-ordinate measuring machines, translation stages, turntables and robot arms. It is difficult to characterize accuracy of positioning systems with multiple degrees of freedom [34, 35, 9]. We therefore adopt a simplified pose error model [31]. As for the sensor, we assume calibration removes systemic errors, leaving

[3]Excepting Prieto [21], grazing angle effects [39, 1, 19, 20] have generally been treated subjectively by giving preference to low grazing angle viewpoints rather than evaluating the objective effects of grazing angle on measurement quality.

```
Acquire rough model by pre-programmed exploration
Decimate the rough mesh model
Segment the rough model by feature type (optional)
While (Unscanned rough model regions)
   Generate optimal candidate viewpoint set
   Compute measurability, form measurability matrix
   Solve the set covering problem, select viewpoints
```

Table 1: Modified Measurability Matrix (3M) Algorithm Pseudo Code

only residual stochastic errors. Errors in sensor position, boresight axis and boresight rotation (twist) are modeled as independent random processes. Position error is modeled as a 3D vector uniformly distributed in direction, whose magnitude is a zero-mean Gaussian process with standard deviation $\sigma_p$. Axis error is modeled by a unit vector uniformly distributed on a cone centered on the boresight whose half-angle is a zero-mean Gaussian process with standard deviation $\sigma_a$. Twist error is modeled as a zero-mean Gaussian process with standard deviation $\sigma_t$. We assume constant pose error statistics but spatially-varying performance can be accommodated. In practical application of our view planning algorithm, this simplified pose error model should be replaced by one tailored to the specific positioning system configuration in use.

### 2.7 Modified Measurability Matrix (3M) Algorithm

Table 1 shows the 3M algorithm in pseudo code.

**Rough Model Acquisition** A rough model is acquired by a rapid, preprogrammed view plan and robust model building techniques [22]. Polygonal meshes are used for their inherent flexibility. The approach to automated rough model acquisition will depend on relative object size and imaging system capabilities. A coarsely sampled view sphere approach [32] would be suitable for objects comparable in size or smaller than the sensor frustum. For large objects, a coarsely sampled space carving technique would be suitable [32].

**Rough Model Decimation** The rough model is decimated [37] to a level just adequate for view planning. This level is experimentally determined for the application domain. Decimation concentrates sampling in high curvature regions, which is of interest both for viewpoint generation and for shape fidelity. Section 4 examines object surface space sampling.

**Rough Model Segmentation** For a given viewpoint, object coverage is limited by the sensor cross-sectional footprint and by occlusion. Segmenting the object surface into patches along the boundaries of major geometric features reduces the net cost of computing $\mathbf{M}$. However, this complexity reduction adds a preprocessing step, may increase view plan length due to patch edge effects and may introduce occlusion estimation errors by localizing view planning to individual surface patches. The technique should be used sparingly. Some objects with distinct edges lend themselves to segmentation (e.g. the mask object shown later), others do not. Segmentation is frequently appropriate for inspection.

**Viewpoint Generation** Candidate viewpoints are generated that are most likely to measure the surface in accordance with the specified criteria. In the simplest case, a candidate generalized viewpoint is created for each surface point which is optimal for that surface point - that is, for each vertex of the rough model. Section 5 describes optimized viewpoint generation.

**Measurability Estimation** Using the input specification and system models, a measurability matrix is computed for the entire rough model or for each surface patch, if segmented. Each element $m_{ij}$ of $\mathbf{M}$ is subject to the frustum occupancy, visibility and specification-compliance tests. For segmented models, visibility analysis is local to the target surface patch.

**Viewpoint Selection** Upon computation of the measurability matrix or matrices, a number of techniques are available to solve the set covering problem (Section 3) to derive a set of viewpoints, the view plan. If the rough model has been segmented, component view plans are merged.

**Summary** The 3M algorithm is specification-based, using objective measurability criteria from experimentally-derived system performance models. Complexity is reduced by optimized, sparse sampling in $S$ and $V$ plus optional segmentation of the problem into smaller components.

## 3 Theoretical Framework

***VPP Solution Landscape*** Pose uncertainty due to positioning system inaccuracy necessitates image-based registration [5], in turn requiring a degree of image overlap i.e. viewpoint correlation. Viewpoint correlation also impacts discretization of viewpoint space.

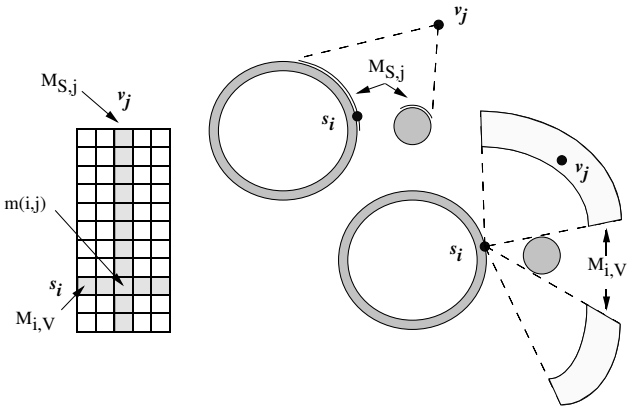


Figure 4: Measurability Matrix Row and Column Vectors

We desire candidate viewpoints sufficiently nearby to satisfy registration and integration requirements yet far enough apart for efficient sampling of viewpoint space. A physics-based VPP set covering algorithm based on this paradigm may be possible.

***Measurability Matrix*** It is instructive to partition $\mathbf{M}$ into column vectors $\mathbf{M}_{S,j}$ and row vectors $\mathbf{M}_{i,V}$. The set $S_j$ of surface elements measurable by viewpoint $\mathbf{v}_j$ is defined by the corresponding column vector $\mathbf{M}_{S,j}$. Similarly, the region $V_i$ of viewpoint space from which surface element $\mathbf{s}_i$ is measurable corresponds to the row vector $\mathbf{M}_{i,V}$. These relationships are illustrated in Figure 4 with 2D slices through an object resembling a coffee cup. Thus, the solution to the VPP is simply to cover the rows of $\mathbf{M}$ with a minimal subset of its columns. Consequently, it is immediately apparent that the VPP is isomorphic to the set covering problem (SCP), a well-studied problem in combinatorial optimization known to be NP-complete [16].

***IP Formulation*** We can then formally express the VPP as the following integer programming (IP) problem [27], where we use IP notation conventions:

$$\text{Minimize } Z = \sum_{j=1}^{v} c_j x_j \text{ , subject to} \tag{6}$$

$$\sum_{j=1}^{v} m_{ij} x_j \geq 1 \; ; \; i = 1, \ldots, s \; , \tag{7}$$

$$c_{kj} \geq x_k x_j \; ; \; k = 1, \cdots, (v-1) \; ; \; j = k+1, \cdots, v \; , \tag{8}$$

$$x_j \in \{0, 1\} \; ; \; j = 1, \ldots, v \; . \tag{9}$$

Equation 9 applies an integer constraint on viewpoint variable $x_j$. $\mathbf{X} = [x_j]$ spans viewpoint space $V$ as sampled by the viewpoint generation stage. The optimal view plan $\mathbf{X}$ is the lowest cost viewplan. In the objective function (Equation 6), coefficient $c_j$ is the movement cost associated with viewpoint $j$. This usage would apply to a positioning system with significant, non-uniform movement costs[4]. Otherwise, movement costs can be set to 1, an easier case known as the unicost SCP [2], the case for experiments reported herein. Equation 7 ensures each row of $\mathbf{M}$ (each surface point) is covered by at least one viewpoint. Equation 8 imposes an image-based registration constraint, where $c_{kj}$ is 1 if a registration path exists between viewpoints $x_k$ and $x_j$ and 0 otherwise. The technique for computing $c_{kj}$ from $\mathbf{M}$ is based on viewpoint correlation [27, 29]. There is no need to include a viewpoint feasibility constraint in the above formulation. It is more efficient to avoid generating infeasible viewpoints.

***Set Covering Algorithms*** Several well-established techniques are available to solve the set covering problem, including simulated annealing [33], genetic algorithm [2], Lagrangian relaxation [8, 10] or other methods [25]. For most reconstruction tasks, we have found that the unsophisticated but fast greedy search algorithm [14] provides good results. View plan lengths are close to the optimal. Marginal view plan inefficiency is offset by improved immunity to various planning and data acquisition errors provided by view plan redundancy. Tasks demanding high view plan efficiency, such as industrial inspection applications involving repetitive view plan execution or some object reconstruction tasks, can employ one of the more efficient but computationally expensive set covering algorithms.

***Computational Complexity*** As a pre-planned activity, physically scanning and building the exploratory model has constant complexity, which is not to say that the time taken for these activities is negligible. The set covering problem is NP-complete but has a variety of sub-optimal solution techniques. Constructing $\mathbf{M}$ is the computational crux. $\mathbf{M}$ has $sv$ elements, where $s = |S|$ is the number of rows (surface

[4] An example is a rotary joint limited to a discrete set of accurate orientations where change requires a unlock-rotate-relock sequence. In some cases, system recalibration may be required upon reconfiguration of a positioning system component.

points) and $v = |V|$ is the number of columns (viewpoints). The most computationally intensive task is visibility analysis. In general, ray tracing is required twice per $m_{ij}$ - once each for the optical source and receiver. Each ray tracing operation involves testing transmit or receive rays with each triangle $t_k$ of the rough model mesh. As the number of triangles $t \approx s$, the complexity of deriving $\mathbf{M}$ is $\mathcal{O}(s^2 v)$. For segmented models, consider (for analysis purposes only) uniform segmentation into $c$ segments. For each segment, $s \rightarrow s/c$ and $v \rightarrow v/c$ due to our viewpoint generation scheme (Section 5). Visibility analysis is local to each segment, equivalent to partitioning the global measurability matrix. Computing one matrix has complexity $\mathcal{O}(s^2 v/c^3)$ and all matrices, $\mathcal{O}(s^2 v/c^2)$.

It is evident that success with measurability matrix algorithms requires sparse sampling of object surface space and viewpoint space. The power of the technique is also immediately apparent for we have, in one data structure, all information necessary to construct an accurate, robust and efficient view plan. This raises important questions, which we address next:

- *How rough can the exploratory model be? (Sec. 4)*
- *How to optimally sample viewpoint space? (Sec. 5)*
- *View plan tolerance to pose uncertainty. (Sec. 6)*

# 4 Sampling Object Surface Space

The required level of model detail has received limited attention in the view planning literature. Tarbox's analysis of sampling density [39] was limited to grazing angle effects. Range imaging is subject to limitations of a sampled representation of a continuous surface, so aliasing effects can be anticipated. Surface sampling density dominates measurability matrix computation and influences estimating accuracy for surface normals, grazing angles and feature visibility.

Experiments [28] have shown a rough model sampling level 32 times lower than the target fine model provides good measurability prediction for deep cavities, a scanning challenge for triangulation-based range cameras, and for natural objects with multiple shadow features. Sampling density can be further reduced for less complex shapes, such as manufactured objects with smoothly flowing lines. The lower bound is constrained by frustum cross-section, pose error and registration/integration overlap requirements. A rule of thumb for the lower bound on rough model sampling density is $A_o/25$ where $A_o$ is the frustum cross-section area at the sensor's optimal stand-off distance.

These experiments also showed that sampling noise as high as $\sigma_{rm} = 0.02 R_{min}$ had only a minor impact. Measurability estimate uncertainty was marginally increased but average measurability was largely unchanged. On average, there was a slight increase in view plan length. This additional scanning cost was offset by improved robustness to other error sources from the more extensive covering of viewpoint space.

These sampling rate and error tolerance levels are suitable initial parameter settings but will require experimental optimization for each imaging environment set-up and class of object shape complexity.

# 5 Sampling Viewpoint Space

**Conventional Schemes** A common stratagem to constrain the high dimensionality of $V$ is to use a virtual, object-centered "view sphere". Almost all view sphere approaches [32] use a fixed stand-off distance such that the sensor frustum encloses the entire object. The strategy does not take sensor performance variability with stand-off distance into account, is a poor match for the mobility envelopes of many positioning systems and fails completely when object size exceeds frustum dimensions.

With few exceptions[38, 20], traditional methods fail to recognize the importance of sensor parameters in addition to pose. Difficult view planning tasks cannot ignore configurable sensor parameters.

Prieto [21] synthesizes optimum viewpoints patch-by-patch by computing surface normals from NURB surfaces in a CAD model. If not occluded from the targeted patch, the viewpoint is set along the surface normal at the optimum stand-off distance, else it is moved until visibility is achieved at a minimal grazing angle. The technique is used to generate view swathes [32] in an inspection application for manufactured parts.

In Lamb's contour following approach [17], pose is constrained by maintaining sensor stand-off so that the surface is centered in the sensor DOF, scanning perpendicularly and minimizing orientation changes. In general, these are mutually exclusive constraints. Soucy's contour following approach [36] is somewhat similar. Both schemes generate view swathes.

**Model-based Viewpoint Generation** To the first order (Equation 1), measurement precision deteriorates quadratically with range and inversely in proportion to the cosine of the grazing angle in the plane of the optical baseline. Optimal precision will therefore be achieved with the camera positioned at mini-

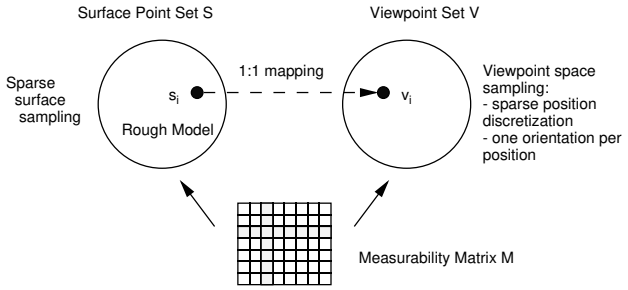


Figure 5: Viewpoint Generation - Optimal Scanning Zone Algorithm

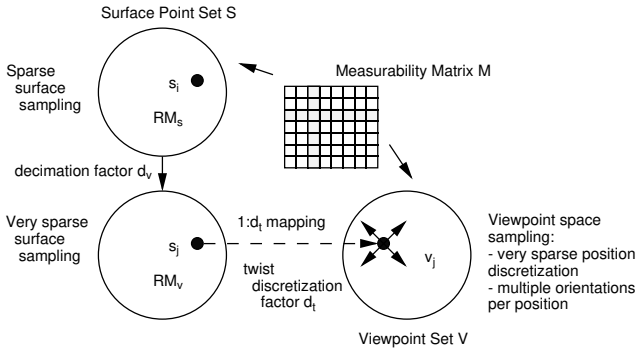


Figure 6: Viewpoint Generation - Decoupled Algorithm

mum range, perpendicular to a targeted surface point, ensuring both incidence and scanning angles are zero. The set of all such viewpoints, corresponding to point-by-point dilation of surface points along their local normals, forms an *optimal viewpoint zone* $\mathbf{S_o}$. $\mathbf{S_o}$ is smooth and well behaved in regions corresponding to planar and convex portions of the object. Depending on surface curvature and stand-off distance, self-intersections may occur in regions corresponding to surface concavities. The local topology of $\mathbf{S_o}$ remains unchanged by dilation. We now describe two viewpoint generation algorithms based on this concept.

**Optimal Scanning Zone Algorithm** An ideal candidate generalized viewpoint $(\mathbf{v}, \lambda_\mathbf{s})$ with pose $\mathbf{v}$ and parameters $\lambda_\mathbf{s}$ is created for each surface point (Figure 5). Each rough model vertex is dilated along the local surface normal by a stand-off distance $f_d R_o$, where $f_d$ is a stand-off adjustment factor and $R_o$ is the optimum scanning range, usually equal to $R_{min}$. $f_d$ is an experimentally-derived constant slightly greater than one to allow for rough model sampling errors. We find $f_d = 1.02$ is a good choice. The dilated vertex becomes the position of the corresponding candidate viewpoint. The viewpoint's axis is set to the negative of the dilation vector. Setting twist orientation is less straightforward as it is influenced by shadow effects arising from object shape over a broader surface region. We have experimented with several different approaches [23]. In one of these, dubbed "variable", sensor twist angle is set to maximize the distance of the receiver from the surface patch to enhance visibility of most features.

We postulate the algorithm provides a near-optimal sampling of $V$ for objects with Lambertian scattering properties[5]. Viewpoint parameters $\lambda_\mathbf{s}$ are optimized for each candidate viewpoint. The optimal scanning zone can be mapped to two dimensions, reducing $V$ to 2D from $6D^+$. With a $1:1$ mapping between $S$ and $V$, computational complexity becomes $\mathcal{O}(\frac{s^3}{c^2})$.

**Decoupled Algorithm** It is useful to decouple discretization of $V$ from $S$. Rough model decimation concentrates vertices in high curvature regions, desirable for conserving shape fidelity and for viewpoint generation. While viewpoint correlation is strongly influenced by object shape, it is evident that sampling of viewpoint space remains highly redundant, suggesting we can afford a further sub-sampling by an additional decimation factor $d_v$, reducing $v$ to $s/d_v$. A further consideration is minimization of shadow effects which are sensitive to sensor twist orientation. Experiments have shown it is difficult to reliably characterize such features to automatically set twist orientation. Sub-sampling the twist component into $d_t$ quantization intervals resolves this problem. Overall computational complexity becomes $\mathcal{O}(\frac{s^3 d_t}{c^2 d_v})$. We find good results are obtained for $d_t/d_v \approx 1$.

The essence of the decoupled algorithm, then, is further decimation of the already coarse rough model for more efficient viewpoint generation. We now use two rough model variants (Figure 6) - one to represent surface geometry and the other for viewpoint generation. The original rough model $RM_s$ remains the basis for sampling surface space and is tied to rows of $\mathbf{M}$. It is further decimated to create $RM_v$ which becomes the basis for viewpoint generation and relates to columns in $\mathbf{M}$. The strategy maintains coarse sampling in $RM_s$ at a level of shape fidelity sufficient for visibility analysis and surface normal estimation. Very sparse sam-

[5]For specular surfaces, imaging geometry is more sensitive and must take the location of both the optical transmitter and receiver into account.

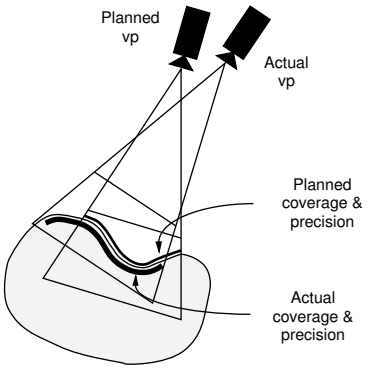


Figure 7: View Planning with Pose Uncertainty

pling in the position component of viewpoint space in $RM_v$ reduces viewpoint correlation to a more efficient level while increased sampling of the twist component of orientation is more robust with respect to object shape complexity and shadow effects.

**Viewpoint Filtering** Collision of the sensor and positioning system with themselves, the object or any other structure in the imaging environment is a concern. Viewpoints violating collision avoidance zones are deleted with the expectation that associated surface regions will be covered by adjacent viewpoints on $\mathbf{S_o}$. Pose constraints due to mobility limitations are applied on a case-by-case basis, mapping the optimum viewpoint to the nearest feasible pose. Excessive mobility constraints will negate the advantages of the proposed viewpoint generation scheme. Finally, configurable sensor parameters are optimized for each candidate viewpoint based on the model specification, system capabilities and rough model surface characterization. For the sensor studied in the present work, one parameter (scan length) is configurable.

**Summary** Our viewpoint generation approach optimizes sampling of $V$ with generalized viewpoints by exploiting a sensor performance model and knowledge of approximate object geometry.

# 6 View Planning with Pose Uncertainty

## 6.1 Pose Error Effects

When a view plan is sent to a positioning system whose accuracy is inferior to the sensor, the coverage of individual viewpoints and the view plan as a whole are compromised. Image coverage, measurement precision, sampling density and feature visibility are effected (Figure 7). We can recover an actual pose estimate post-facto with suitable registration techniques and subsequently re-estimate measurement quality. However, the process is still left with data acquisition differing from that which had been planned. As pose error deteriorates, the computationally intensive view planning phase is progressively compromised - ultimately to be rendered futile. Consequently, there is a need to make the process robust to pose error.

Our analytical and experimental examination of pose error effects on range sensing [31, 30] has shown the phenomena to be complex. Pose position error effects on a single view are minor. Pose twist orientation errors are amplified by the length of the sensor baseline but their impact is also minor at anticipated error levels. Axis orientation error is particularly troublesome as the effects are amplified by standoff range. Due to view plan redundancy, partial-to-complete masking of pose error effects is found at low error levels, followed by a rapid decrease in average measurability and rapid increase in measurability variance with pose error deterioration. As coverage failure in reconstruction and inspection tasks implies costly rework, such unpredictability may be unacceptable.

## 6.2 Pose Error Compensation

The problem of pose error effects and their compensation has received scant attention. Tarabanis et al [38] use a synthesis approach for generalized viewpoints which seeks to centralize viewpoints in the admissible domain. Tarbox [39] uses morphological erosion of viewpoints on the periphery of viewpoint sets to reduce pose error vulnerability. While useful, neither approach is based on objective performance criteria nor the actual error mechanisms.

Pose error impacts all three measurability tests - frustum occupancy, visibility and specification compliance. Within expected pose error levels, frustum occupancy is degraded the most, while the impact on the other measurability tests is minor.

Two mechanisms can mitigate pose error effects - view plan redundancy and conservative adjustments to the estimation processes for frustum occupancy, specification compliance and visibility. View plan redundancy has a major mitigating effect. As a consequence, view plans for objects with complex geometry are less vulnerable to pose error because shape complexity drives up view plan redundancy. The reverse is true for objects with simple geometric shape.

Our pose error compensation scheme [24] operates

at the measurability matrix computation stage for the exploratory model. It compensates for error in estimating frustum occupancy and specification compliance by substituting more conservative test parameters[6]. The adjustments are based on a statistical analysis of pose error effects [31] for the applicable imaging environment. These parameters are modified by a user-selected percentage compensation factor. The compensation factor is generally set at a low value, typically 10% - 40%, to maintain view plan efficiency. Too high a compensation value unnecessarily drives up view plan length. The approach is a beneficial tradeoff between statistically-based measurability parameter adjustment and view plan redundancy naturally associated with object shape complexity.

As results in the next section illustrate, the compensation scheme improves view planning performance for a given view plan by raising the expected value of measurability to almost the pose-error-free case and by reducing measurability variance. Pose error compensation is particularly advantageous for inspection, which usually involves multiple executions of a single view plan. The technique is also useful for reconstruction but results will be less predictable as the view plan is normally executed only once. Appropriate system design should specify positioning system performance compatible with the target measurement precision and sampling density goals. Pose error compensation can then be applied to further mitigate pose error effects.

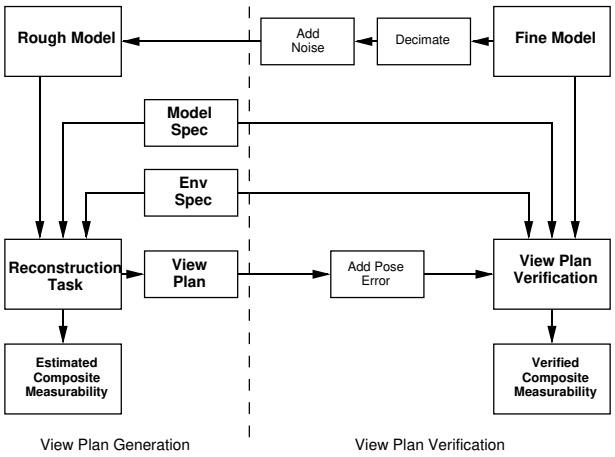


Figure 8: Experimental Process - Measurability Verification

| Specification | Sensor 1 | Sensor 2 |
|---|---|---|
| XZ-plane FOV ($\Phi_x$) | 27° | 24° |
| Optical baseline ($b$) | $180mm$ | $100mm$ |
| Min range ($R_{min}$) | $142mm$ | $205mm$ |
| Max range ($R_{max}$) | $407mm$ | $265mm$ |
| YZ-plane max scan ($L_y$) | $300mm$ | $200mm$ |
| Max image size (rangels) | 256x256 | 1024x1024 |

Table 2: Range Sensor Specifications

# 7 Experimental Results

***Experimental Process*** Our approach to examining the view planning problem has been to use a high fidelity closed loop simulation of the environment. The experimental process (Figure 8) begins with a model specification, an imaging environment specification (range camera and positioning system) and a detailed object model acquired by a high performance range camera. To simulate rough model acquisition, the fine model is decimated and sampling noise is optionally added. A view plan is then computed by the 3M algorithm based on the rough model, model specification and environment specification. The derived view plan is optionally corrupted with pose error. The loop is subsequently closed by executing the noisy view plan against the original fine model. Finally, performance measures are computed.

[6]We do not presently make allowance for the impact of pose error on visibility estimation, but this could be added without difficulty.

We have chosen to concentrate on the rough model to fine model stage, believing this to be the crux of specification-driven view planning. The simulation method was chosen for its ability to explore the subject matter extensively by conducting a large number of experiments with full control and access to system parameters. A variety of existing techniques are available to acquire an approximate object model at the scene exploration stage [32].

Two experiments are reported to demonstrate the 3M algorithm. The experiments examine two range cameras with different capabilities, different model specifications, two objects presenting difficult scanning challenges and two viewpoint generation schemes with the added dimensions of rough model approximation error, pose error and pose error compensation. In other work, we examine rough model approximation error [28], pose error effects [30, 31] and pose error compensation [24] in greater detail.

Both modeled range cameras (Table 2) are line-scan configurations but use different range measurement technology. Sensor 1 is an early generation commer-

Figure 9: Tsimshian Stone Mask

| View Plan | Comp. | Measur. (average) | Measur. (std dev) |
|---|---|---|---|
| $n_{Best} = 5$ | 0% | $\overline{m_v} = 0.9523$ | $\sigma_{m_v} = 0.0120$ |
| $n_{gs} = 7$ | 0% | $\overline{m_v} = 0.9664$ | $\sigma_{m_v} = 0.0123$ |

Table 3: Verified Measurability - Mask with Pose Error, no Compensation

| View Plan | Comp. | Measur. (average) | Measur. (std dev) |
|---|---|---|---|
| $n_{Best} = 5$ | 35% | $\overline{m_v} = 0.9642$ | $\sigma_{m_v} = 0.0114$ |
| $n_{gs} = 7$ | 35% | $\overline{m_v} = 0.9795$ | $\sigma_{m_v} = 0.0066$ |

Table 4: Verified Measurability - Mask with Pose Error Compensation

cial Biris scanner characterized by a large optical baseline and depth of field. In comparison, sensor 2, an early generation autosynchronized scanner, exhibits a shorter optical baseline, narrower depth of field and larger range image size. These technologies are described at www.vit.iit.nrc.ca/VIT.html.

***Variable Algorithm*** The Tsimshian stone mask[7] (Figure 9), carved from stone in the form of a thick shell, is a case where segmentation is advantageous. A high quality model acquired by the NRC colour range camera was decimated to a lower resolution mesh ($s = 244$) and partitioned into front and back segments. Featuring smaller cavities and ridges within the main steep-walled cavity, the rear segment presented a difficult view planning challenge for sensor 1's long baseline. The specification called for 50 $\mu m$ and 2 $s/mm^2$. Surface sampling noise was not added in the trials reported here but pose error was introduced for a second set of experiments. The "variable" viewpoint generation algorithm was used (Section 5).

In the absence of sampling or pose errors, the view plan of size $n_{gs} = 7$ computed by the variable algorithm with greedy search produced verified measurability of $m_v = 0.9807$ with respect to the specified goals. The shortest view plan found by the probing method [25] (size $n_{Best} = 5$) gave $m_v = 0.9663$. The efficiency of these plans is $e_v = 0.714$ and $e_v = 1.0$, respectively. Figure 10 presents the verified measurability covering for the more efficient view plan. The left column shows measurability projections along the camera boresight for individual viewpoints while cumulative measurability projections are shown on the right from an orthogonal perspective. For display conventions, see Section 2.4. All surface points are measured within specification excepting a few spots on the steep side walls of the main cavity beyond the reach of this long baseline sensor. These results are comparable to what a skilled operator could achieve.

Next, the computed view plan was corrupted by pose error using the model described in Section 2.6. Table 3 shows average and standard deviation verified measurability in the presence of pose error ($\sigma_p = 3\% R_{min} = 4.26mm$, $\sigma_a = \sigma_t = 3°$) without pose error compensation. Table 4 shows the impact of compensation for the same level of pose error. In both cases, twenty trials were conducted. Compensation allows us to recover, on average, almost the same level of measurement performance in the absence of pose error.

***Decoupled Algorithm*** The second test object, the well known bunny (Figure 11 (a)), presents a challenge from difficult self-occlusion problems in the vicinity of closely-spaced, large protuberances (the ears). Less obvious, but just as difficult, are subtle shadowing problems around a variety of folds and creases in the bunny's fur as well as small crevices around the legs, feet, chin, ears and tail. Sensor 2's shallow depth of field presents an additional planning challenge. The model specification called for 40 $\mu m$ and 10 $s/mm^2$. Segmentation was not used and view plans were computed for the object as a whole. Viewpoints were generated by the "decoupled" algorithm previously described at Section 5. A rough model ($|RM_s| = 702$) captured the complex shape and was further deci-

[7]The Tsimshian stone mask is a masterpiece of northwest coast art in the collection of the Canadian Museum of Civilization (VII-C-329). It was collected at the Tsimshian village of Kitkatla in 1879 by I.W. Powell.

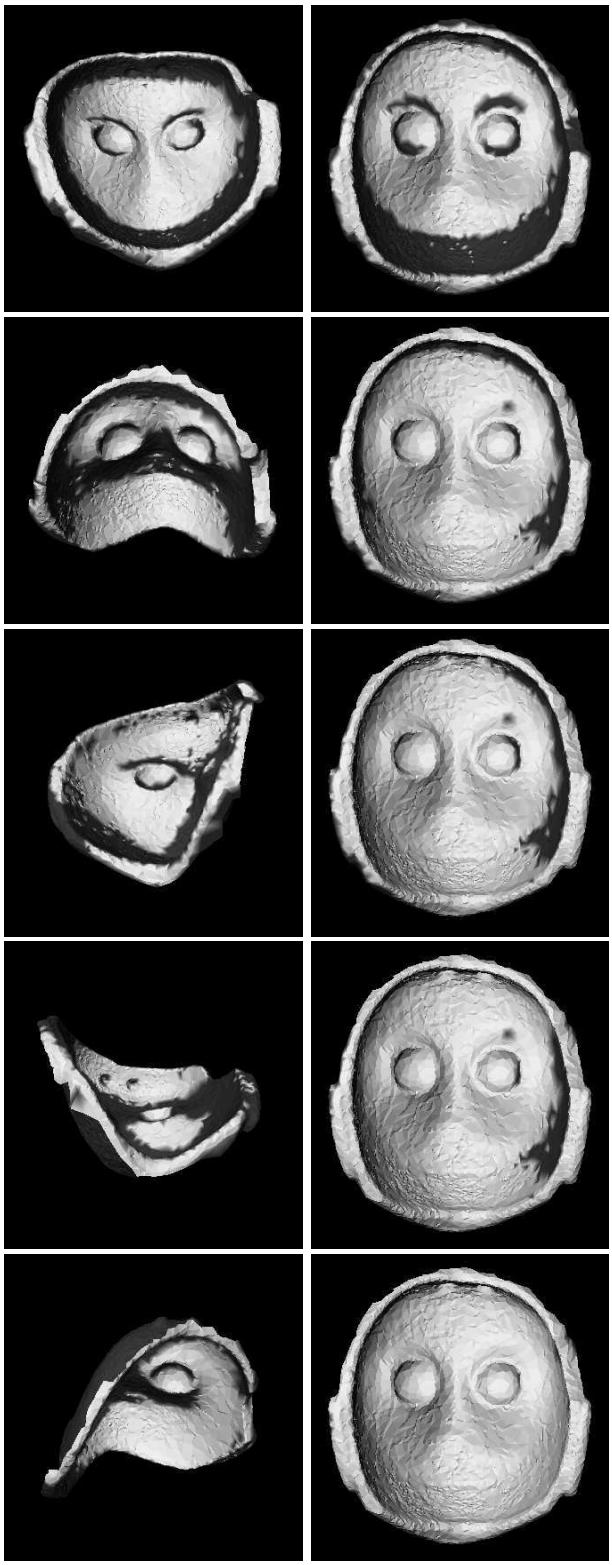

Figure 10: Verification of Tsimshian Mask View Plan
Left - Individual Viewpoint Measurability Projections - Camera Boresight View
Right - Cumulative Measurability Projections - Orthogonal View

Figure 11: Bunny Models: (a) High Resolution Model, (b) Noisy $RM_s$, (c) Noisy $RM_v$

| **View Plan** | **Comp.** | **Measur. (ave)** | **Measur. (std dev)** |
|---|---|---|---|
| $n_{Best} = 16$ | 0% | $\overline{m_v} = 0.9978$ | $\sigma_{m_v} = 0.0029$ |
| $n_{Best} = 16$ | 40% | $\overline{m_v} = 0.9992$ | $\sigma_{m_v} = 0.0011$ |

Table 5: Verified Measurability - Bunny with Pose Error Compensation

mated to $|RM_v| = 72$ for viewpoint generation. The twist component of viewpoint orientation was quantized in $d_t = 10$ intervals of 36°.

In a baseline experiment without sampling or pose errors, the shortest view plan found by the probing method (size $n_{Best} = 16$) produced verified measurability $m_v = 1.0$, $e_v = 1.0$ while the greedy search view plan of size $n_{gs} = 18$ gave $m_v = 1.0$, $e_v = 0.889$.

Next, sampling noise $0.3\%R_{min} = 0.615mm$ was added, giving the rough models a noticeably crumbled appearance (Figure 11 (b) and (c)). Pose error was not added at this stage. The decoupled algorithm produced view plans of $n_{gs} = 20$ with $m_v = 1.0$, $e_v = 0.8$ and size $n_{Best} = 16$ with $m_v = 0.9993$, $e_v = 1.0$. While less efficient, it can be seen that redundancy inherent with greedy search set covering protects against modest levels of rough model sampling error.

Maintaining sampling error, we next added pose error $\sigma_p = 6.15mm$, $\sigma_a = \sigma_t = 3°$. Table 5 shows verified measurability statistics for a constant view plan length $n = 16$ at these levels of sampling and pose error, with and without pose error compensation. Compensation recovers average measurability to the pose error free case and reduces measurability variance.

Figures 12 and 13 present one trial of the verified measurability covering for the most efficient view plan ($n_{Best} = 16$) in the presence of surface error and pose error at the levels described plus pose error compensation. As before, individual shaded measurability projections are shown on the left while cumulative measurability projections along the principal axes are

shown on the right. It will be seen that most of the object is measured within approximately half of the view plan, with the remainder addressing small, difficult to measure patches. In this trial, all surface points were measured within specification with the exception of one vertex in the nap of the neck, giving $m_v = 0.9999$. The statistical performance of 40 trials in this series is shown in Table 5. These results are also comparable to what a skilled operator could achieve.

***Computational Efficiency*** The 3M algorithm computed view plans for the mask rear segment in 3.6 minutes and the bunny object in 28.1 minutes, running on a 2.6 GHz Pentium 4 PC. Computing the measurability matrix is the dominant process. These times are well within our goal [32] of producing a specification-compliant plan for a moderately complex object within one hour. Coded in C++, the present research implementation emphasizes robustness and flexibility. Substantial improvement would be achievable with production code efficiencies, more narrowly-specified functionality and with parallelization, as the algorithm is inherently parallelizeable.

***3M Algorithm Evaluation*** We now evaluate the 3M algorithm with respect to the criteria specified in the introduction. Other contemporary techniques have been similarly evaluated at [32].

- **Model specification** Quantified precision and sampling density requirements are imposed in a model specification for the view planning task.
- **Generalizable algorithm** The method is applicable to any triangulation-based active range sensor and positioning system whose performance can be mathematically modeled.
- **Generalized viewpoints** Generalized viewpoints are optimized at the viewpoint generation stage prior to measurability matrix computation. Parameters are defined as fixed or configurable, with nominal values and limits. For comparable computational complexity, experiments show that performance of the decoupled algorithm is superior to the variable algorithm, particularly for natural objects with randomly-oriented shadow features.
- **View Overlap** We use a viewpoint correlation constraint, equivalent to an image overlap constraint. Image overlap is a necessary but not sufficient condition for registration. For completeness, the constraint should also require sufficient shape complexity in the overlap region and incorporate measurement uncertainty. Note, however, that view plans for most objects of interest have such inherent redundancy that the registration constraint is rendered moot.
- **Robust** Several features contribute to robustness i.e. multi-stage problem solving, sensor and positioning system performance models, tolerance of surface sampling errors at the exploratory phase and pose error countermeasures. However, measurement challenges remain, notably specular reflectance and other sensing artifacts.
- **Efficient** The rough-to-fine modeling portion of the present experimental configuration meets the one hour processing objective and is amenable to further speed-up. However, rough modeling processes remain to be fully implemented and integrated in the experimental system.
- **Self-terminating** A variety of self-terminating set covering algorithms can be utilized. For many applications, a simple greedy search process provides a good compromise between view plan efficiency and overall error tolerance.
- **Limited a priori knowledge** The only prior object knowledge required is approximate object bounding dimensions and centroid.
- **Shape constraints** The approach is effective with a wide range of object shapes. Empirically-derived rules of thumb have been provided for rough model sampling rates and error tolerance.
- **Material constraints** The current work assumes objects characterized by Lambertian scattering. Dropouts and outliers resulting from limited sensor dynamic range remain an important open issue. Sensor improvements will help but not eliminate the problem. Further improvements should be possible by incorporating reflectance measurement and modeling in the scene exploration stage, which could also address other error sources.
- **Frustum** The sensor frustum (DOF, FOV and scan length/arc) is modeled.
- **Shadow effect** The sensor model specifies the optical baseline. Visibility is computed from both the laser source and receiver.
- **Measurement performance** Measurability estimation error is low. Good results are obtained with coarse rough model sampling. The most important first-order sensing phenomena are addressed - measurement variation within the frustum and surface inclination effects. However, important sensing artifacts remain, notably geometric and reflectance step edges and multiple reflections. Methods to deal with geometric step edges include "space-time" processing [12] and more sophisticated low level sensor signal processing. Object reflectance modeling [18] has the potential to handle reflectance step edges and multiple reflections.

Figure 12: Verification of Bunny View Plan: Views 1-8
Left - Individual Viewpoint Measurability Projections - Camera Boresight View
Right - Cumulative Measurability Projections: +x, -x, +y, -y, +z, -z axes

Figure 13: Verification of Bunny View Plan: Views 9-16
Left - Individual Viewpoint Measurability Projections - Camera Boresight View
Right - Cumulative Measurability Projections: +x, -x, +y, -y, +z, -z axes

• **6D Pose** The algorithm provides a near-optimal sampling of 6D pose space.
• **Pose Constraints** Pose constraints are applied on viewpoint generation.
• **Positioning system performance** Pose error is modeled over the imaging workspace, with optional pose error compensation. For production use, the current generic pose error model should be replaced by one tailored to the specific configuration in use.

# 8 Conclusion and Future Work

**Summary** The 3M method meets the specified view planning requirements for automated object reconstruction or inspection with the exception of material reflectance properties, aspects of the overlap requirement and some range camera artifacts.

In the work reported in this paper, rough model acquisition for object reconstruction has been simulated for closed-loop performance evaluation. A CAD model is a given for inspection applications. We believe the computational cost of this preliminary phase is reasonable for high performance reconstruction applications, but it is not negligible. A multi-sensor fusion approach may be advantageous - using a fast, wide field-of-view, low precision sensor for scene exploration and collision avoidance in combination with a high quality range sensor for precise surface measurements.

The current work addresses open issues as follows:
• Accuracy is addressed through a quantified specification of model quality objectives, modeling of camera and positioning system performance, and by exploitation of approximate geometric knowledge in an initial exploratory scene model.
• Robustness is addressed by the foregoing as well as pose error compensation and tolerance to rough modelling errors.
• Efficiency is addressed by multi-stage problem solving, sparse and optimal discretization of surface and viewpoint spaces and optional rough model segmentation. Additionally, the 3M algorithm is inherently parallelizable.

The algorithm can provide accurate and robust view planning for automated object reconstruction or inspection applications with high quality sensing objectives using triangulation-based active range cameras on objects characterized by Lambertian scattering. The technique is generalizable for common range camera and positioning system designs and could be extended to handle sensor dynamic range limitations and a variety of sensing artifacts.

**Open Issues and Future Research** The capabilities and limitations discussed above point to remaining open issues in view planning. There are a number of ways in which the sophistication of the sensor model could be improved, which would address several outstanding issues.
(1) *Accuracy and robustness*
- Measure and model object reflectance to handle shiny objects and compensate for the limited dynamic range of range cameras.
- Avoid or compensate for geometric step edges, reflectance step edges and multiple reflections.
(2) *Efficiency*
- Fast and efficient techniques for acquiring a rough scene model.
- Fine tune discretization schemes in surface and viewpoint space.
- Tune the performance of set covering algorithms to the data characteristics associated with the view planning problem.
- Automate surface segmentation for view planning.
- Develop performance benchmarks for objective comparison of view planning algorithm performance.
(3) *Theory*
- Develop a theory for optimal discretization of surface and viewpoint space.
- Extend the theory to include shape complexity in the overlap constraint.

# References


[1] J. Banta and M. Abidi. Autonomous placement of a range sensor for acquisition of optimal 3D models. In *Proc. IEEE 22nd Int. Conf. on Industrial Electronics, Control and Instrumentation, Taipei, Taiwan*, pages 1583–1588, August 5-10 1996.

[2] J. Beasley and P. Chu. A genetic algorithm for the set covering problem. *European Journal of Operational Research*, 94:392–404, 1996.

[3] J.-A. Beraldin, S. El-Hakim, and L. Cournoyer. Practical range camera calibration. In *Proc. Videometrics II, SPIE, Boston, Massachusetts*, volume 2067, pages 21–30, 9-10 September 1993.

[4] P. Besl. Range image sensors. In J. Sanz, editor, *Advances in Machine Vision*. Springer-Verlag, New York, 1989.

[5] P. Besl and N. McKay. A method for registration of 3D shapes. *IEEE Trans. PAMI*, 14(2):239–256, February 1992.

[6] F. Blais. Review of 20 years of range sensor development. *Journal of Electronic Imaging*, 13(1):231–243, 2004.

[7] F. Blais, M. Rioux, and J.-A. Beraldin. Practical considerations for a design of a high precision 3D laser scanning system. In *Proc. SPIE Conf. Optomechanical and Electro-Optical Design of Industrial Systems, Dearborn, Michigan*, volume 959, pages 225–246, 28-29 June 1988.

[8] A. Caprara, M. Fischetti, and P. Toth. Algorithms for the set covering problem. *Annals of Operations Research*, 98:353–371, 2000.

[9] P. Cauchick-Miguel, T. King, and J. Davis. CMM verification: A survey. *Measurement*, 17(1):1–16, 1996.

[10] S. Ceria, P. Nobili, and A. Sassano. A lagrangian-based heuristic for large-scale set covering problems. *Mathematical Programming*, 81:215–228, 1998.

[11] C. Cowan and P. Kovesi. Automatic sensor placement from vision task requirements. *IEEE Trans. PAMI*, 10(3):407–416, May 1988.

[12] B. Curless and M. Levoy. Better optical triangulation through space-time analysis. In *SIGGRAPH '96*, pages 1–10, 1996.

[13] S. El-Hakim and J.-A. Beraldin. Configuration design for sensor integration. In *Proc. Videometrics IV, SPIE, Philadelphia, Pennsylvania*, volume 2598, pages 274–285, 25-26 October 1995.

[14] M. Fisher and L. Wolsey. On the greedy heuristic for covering and packing problems. *SIAM Journal of Algebraic and Discrete Methods*, 3(4):584–591, Dec 1982.

[15] M. Garcia, S. Velazquez, and A. Sappa. A two-stage algorithm for planning the next view from range images. In *British Machine Vision Conference 1998*, pages 720–729, 1998.

[16] T. Grossman and A. Wool. Computational experience with approximation algorithms for the set covering problem. *European Journal of Operational Research*, 101:81–92, 1997.

[17] D. Lamb, D. Baird, and M. Greenspan. An automation system for industrial 3D laser digitizing. In *2nd Int. Conf. on 3D Digital Imaging and Modeling, Ottawa*, pages 148–157, October 4-8 1999.

[18] T. Machida, H. Takemura, and N. Yokoya. Dense estimation of surface reflectance parameters by selecting optimum illumination conditions. In *14th Int. Conf. on Vision Interface, Ottawa*, pages 244–251, 2001.

[19] N. Massios and R. Fisher. A best next view selection algorithm incorporating a quality criterion. In *British Machine Vision Conference 1998*, pages 780–789, September, 1998.

[20] R. Pito. A solution to the next best view problem for automated surface acquisition. *IEEE Trans. PAMI*, 21(10):1016–1030, October 1999.

[21] F. Prieto, R. Lepage, P. Boulanger, and T. Redarce. A cad-based 3d data acquisition strategy for inspection. *Machine Vision and Applications*, 15:76–91, 2003.

[22] G. Roth and W. Wibowo. An efficient volumetric method for building closed triangular meshes from 3D image and point data. In *Proc. Graphics Interface Conf. 97*, May 1997.

[23] W. Scott. *Performance-Oriented View Planning for Automated Object Reconstruction*. PhD thesis, Univ. of Ottawa, 2002.

[24] W. Scott. Pose error compensation for performance-oriented view planning. Technical Report NRC-47175, National Research Council of Canada, Institute for Information Technology, August 2004.

[25] W. Scott. Probing view plan solution space. Technical Report NRC-47447, National Research Council of Canada, Institute for Information Technology, April 2005.

[26] W. Scott, G. Roth, and J.-F. Rivest. Performance-oriented view planning for automatic model acquisition. In *31st Int. Sym. on Robotics, Montreal*, pages 314–319, May 2000.

[27] W. Scott, G. Roth, and J.-F. Rivest. View planning as a set covering problem. Technical Report NRC-44892, National Research Council of Canada, Institute for Information Technology, August 2001.

[28] W. Scott, G. Roth, and J.-F. Rivest. View planning for multi-stage object reconstruction. In *14th Int. Conf. on Vision Interface, Ottawa*, pages 64–71, June 2001.

[29] W. Scott, G. Roth, and J.-F. Rivest. View planning with a registration constraint. In *3rd Int. Conf. on 3D Digital Imaging and Modeling, Quebec City*, pages 127–134, May 2001.

[30] W. Scott, G. Roth, and J.-F. Rivest. View planning with positioning system error. Technical Report NRC-44195, National Research Council of Canada, Institute for Information Technology, May 2001.

[31] W. Scott, G. Roth, and J.-F. Rivest. Pose error effects on range sensing. In *15th Int. Conf. on Vision Interface, Calgary*, pages 331–338, May 2002.

[32] W. Scott, G. Roth, and J.-F. Rivest. View planning for automated 3D object reconstruction and inspection. *ACM Computing Surveys*, 35(1):64–96, March 2003.

[33] S. Sen. Minimal cost set covering using probabilistic methods. In *ACM Sym. Applied Computing, Indianapolis*, pages 157–164, 1993.

[34] Y. Shin and Y. Wei. A statistical analysis of positional errors of a multi-axis machine tool. *Precision Engineering*, 14(3):139–146, July 1992.

[35] J. Soons, F. Thomas, and P. Schellekens. Modeling the errors of multi-axis machines: A general methodology. *Precision Engineering*, 14(1):5–19, July 1992.

[36] G. Soucy, F. Callari, and F. Ferrie. Uniform and complete surface coverage with a robot-mounted laser rangefinder. *Proc. IEEE/RSJ Int. Conf. on Intelligent Robots and Systems, Victoria, B.C., Canada*, pages 1682–1688, October 1998.

[37] M. Soucy and D. Laurendeau. Multi-resolution surface modeling from multiple range views. In *Proc. IEEE Conf. Vis. Pat. Rec.*, pages 348–353, June 1992.

[38] K. Tarabanis, R. Tsai, and P. Allen. The MVP sensor planning system for robotic vision tasks. *IEEE Trans. Robotics and Automation*, 11(1):72–85, February 1995.

[39] G. Tarbox and S. Gottschlich. Planning for complete sensor coverage in inspection. *Computer Vision and Image Understanding*, 61(1):84–111, January 1995.